Laser-Controlled Real- and Reciprocal-Space Topology in Multiferroic Insulators

Tomoki Hirosawa,[1,2] Jelena Klinovaja,[2] Daniel Loss,[2] and Sebastián A. Díaz[2,3]
[1]Department of Physics, University of Tokyo, Bunkyo, Tokyo 113-0033, Japan
[2]Department of Physics, University of Basel, Klingelbergstrasse 82, CH-4056 Basel, Switzerland
[3]Faculty of Physics, University of Duisburg-Essen, 47057 Duisburg, Germany

(Received 12 October 2021; revised 2 December 2021; accepted 17 December 2021; published 20 January 2022)

Magnetic materials in which it is possible to control the topology of their magnetic order in real space or the topology of their magnetic excitations in reciprocal space are highly sought after as platforms for alternative data storage and computing architectures. Here we show that multiferroic insulators, owing to their magnetoelectric coupling, offer a natural and advantageous way to address these two different topologies using laser fields. We demonstrate that via a delicate balance between the energy injection from a high-frequency laser and dissipation, single skyrmions—archetypical topological magnetic textures—can be set into motion with a velocity and propagation direction that can be tuned by the laser field amplitude and polarization, respectively. Moreover, we uncover an ultrafast Floquet magnonic topological phase transition in a laser-driven skyrmion crystal and we propose a new diagnostic tool to reveal it using the magnonic thermal Hall conductivity.

DOI: 10.1103/PhysRevLett.128.037201

Historically, manipulating the magnetic order in solids has led to reliable and widely used data storage devices [1]. The recent mainstream embrace of topology as a powerful guiding principle in condensed matter combined with the growing need for alternative platforms for conventional as well as unconventional computing have reinvigorated magnetism research. For instance, magnetic textures whose real-space topology provides them with enhanced stability have garnered attention as potential information carriers in future logic devices and novel, alternative computing architectures [2–4]. Magnons, the quanta of spin waves supported by magnetic materials, can also become topological but in reciprocal space [5–9]. Dictated by the bulk-boundary correspondence, bulk topological magnons can result in robust, unidirectional magnonic currents propagating along the sample edges which have been proposed as information conduits for magnonics [10,11]. So far, the study of topological magnetic textures in real space and topological magnons in reciprocal space have developed independently. Therefore, having a single platform capable of supporting both topologies is highly desirable as it can facilitate research on their combined phenomena, and potentially lead to applications that exploit their unique functionalities either simultaneously or selectively.

Among the family of materials that can support magnetic textures and magnons with nontrivial topology, electrically insulating magnets stand out because they are exempt from Joule heating [12,13]. This technologically advantageous property, however, brings about the challenge of controlling magnetism besides the standard approach based on electric currents [14]. One natural and promising route is to use the electromagnetic field from high-frequency lasers, which can also allow noncontact, ultrafast manipulation [15–20]. Controlling magnetic textures, and hence magnons, with lasers can be accomplished in multiferroics whose general spin lattice Hamiltonian is given by

$$H(t) = H_0 - \sum_{\boldsymbol{r}} g\mu_B \mathbf{B}(t) \cdot \boldsymbol{S}_{\boldsymbol{r}} - \mathbf{E}(t) \cdot \mathbf{P}_{\boldsymbol{r}}, \qquad (1)$$

where $\boldsymbol{S}_{\boldsymbol{r}}$ is the classical spin vector at site $\boldsymbol{r}$, g and μ_B respectively denote the g factor and Bohr magneton, and H_0 is the Hamiltonian in the absence of laser irradiation. Here $H(t+T_0) = H(t)$ with $T_0 = 2\pi/\omega_0$ denoting the period of the laser electromagnetic field at frequency ω_0.

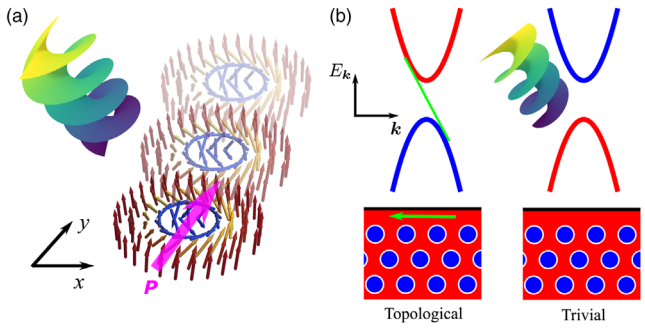

FIG. 1. Real- and reciprocal-space topology can be controlled by lasers. (a) The topological spin structure of a skyrmion carrying in-plane electric polarization $\mathbf{P}$ undergoes translational motion under a circularly polarized laser. (b) An ultrafast topological phase transition occurs in the Floquet magnon band structure of skyrmion crystals due to the effective magnetic field induced by circularly polarized laser irradiation.

Multiferroics not only interact with the magnetic field $\mathbf{B}(t)$ from the laser. Thanks to their magnetoelectric coupling their electric dipole moment $\mathbf{P}_r$, induced by the magnetic order, also interacts with the electric field $\mathbf{E}(t)$ [21–24]. This coupling gives rise to new phenomena and potential functionalities that are not possible just with oscillating magnetic fields.

Here we show that a high-frequency laser, in the terahertz range, can be used to control topological magnetic textures and Floquet topological magnons of multiferroic insulators. A prime example of noncollinear magnetic textures with nontrivial topology in real space is skyrmions [25]. We uncover a novel mechanism that sets skyrmions into motion [see Fig. 1(a)] where, unlike previous proposals, there is no need to tune the laser frequency to be at resonance with internal skyrmion magnon modes [26–29]. The magnon bands supported by a static skyrmion crystal can also be topological in reciprocal space [30–35]. We show that a topological phase transition in the Floquet magnon spectrum can be driven by a terahertz laser [see Fig. 1(b)]. The topological phase reveals itself through robust, chiral magnonic edge states guaranteed by the bulk-boundary correspondence. Furthermore, we establish that the magnonic thermal Hall conductivity [5,36–38], a bulk coefficient, carries a signature of this topological phase transition and thus can be used as a diagnostic tool. For the above phenomena to occur, we find dissipation to be of crucial importance [39]. To consistently incorporate dissipative effects into our description, thus circumventing the issue of reaching a thermal state at long times, we adopt the Floquet-Magnus expansion for classical systems [40], and extend the Floquet magnon formalism to multiferroics with a time-dependent, noncollinear magnetic unit cell.

Model.—Inspired by the vast body of available experimental characterization, we use a model that closely describes the multiferroic insulator Cu_2OSeO_3 [41–43], which is known to host skyrmions as isolated objects as well as in crystalline form, hence an ideal test bed for our predictions.

Considering a thin film sample, the spin lattice Hamiltonian is defined on a square lattice as [44–46]

$$H_0 = \frac{1}{2}\sum_{\langle \boldsymbol{r},\boldsymbol{r}'\rangle}(-J_{\boldsymbol{r},\boldsymbol{r}'}\boldsymbol{S}_{\boldsymbol{r}}\cdot\boldsymbol{S}_{\boldsymbol{r}'} + \boldsymbol{D}_{\boldsymbol{r},\boldsymbol{r}'}\cdot\boldsymbol{S}_{\boldsymbol{r}}\times\boldsymbol{S}_{\boldsymbol{r}'}) - g\mu_B B_0\sum_{\boldsymbol{r}}\boldsymbol{S}_{\boldsymbol{r}}\cdot\hat{\boldsymbol{z}}. \tag{2}$$

The nearest-neighbor spins interact via ferromagnetic exchange $J_{\boldsymbol{r},\boldsymbol{r}'} = J(\delta_{\boldsymbol{r}-\boldsymbol{r}',\pm a\hat{\boldsymbol{x}}} + \delta_{\boldsymbol{r}-\boldsymbol{r}',\pm a\hat{\boldsymbol{y}}})$, with $J>0$ and a is the lattice constant, and Dzyaloshinskii-Moriya interaction $\boldsymbol{D}_{\boldsymbol{r},\boldsymbol{r}'} = D(\boldsymbol{r}-\boldsymbol{r}')/|\boldsymbol{r}-\boldsymbol{r}'|$. In what follows, $\boldsymbol{S}_{\boldsymbol{r}} = S\boldsymbol{m}_{\boldsymbol{r}}$ is the total magnetization at site $\boldsymbol{r}$ with $\boldsymbol{m}_{\boldsymbol{r}}$ denoting a unit vector and $S=1$ for each Cu-ion tetrahedra [45]. The spins also couple to an applied static magnetic field $\mathbf{B}_0 = B_0\hat{\boldsymbol{z}}$.

In Cu_2OSeO_3, a noncollinear spin texture induces a local electric polarization via the d-p hybridization mechanism [23,42,45] and whose explicit form depends on the direction of the applied static magnetic field relative to the crystallographic axes. Orienting the sample such that $\mathbf{B}_0 \| [110]$, the local electric dipole moment is given by [42,45]

$$\mathbf{P}_{\boldsymbol{r}} = \lambda\left(-m_{\boldsymbol{r},x}m_{\boldsymbol{r},y}, \frac{-m_{\boldsymbol{r},x}^2 + m_{\boldsymbol{r},z}^2}{2}, m_{\boldsymbol{r},y}m_{\boldsymbol{r},z}\right), \tag{3}$$

thus inducing a total electric polarization along the y axis and where the magnetoelectric coupling strength is $\lambda = 5.64\times10^{-27}$ μCm.

The time-periodic driving fields in Eq. (1) are introduced as $\mathbf{E}(t) = E_d\{\sin(\omega_0 t+\delta), \cos(\omega_0 t), 0\}$ and $\mathbf{B}(t) = B_d\{\cos(\omega_0 t), -\sin(\omega_0 t+\delta), 0\}$ with $B_d = E_d/c$ and c denoting the speed of light. The laser polarization is determined by δ, with $\delta = 0,\ \pi/2,\ \pi$ corresponding to right-circularly polarized (RCP), linearly polarized, and left-circularly polarized (LCP) light, respectively. In Table I, we summarize the conversion between dimensionless parameters and physical units for this model.

TABLE I. Unit conversion table for $J=1$ meV, $D/J=0.09$ and $a=0.5$ nm [43]. Physical variables are obtained by multiplying the dimensionless variables on the middle column by the values on the right column.

	Dimensionless	Physical unit
Time	$\bar{t} = \hbar t/JS$	≈0.66 ps
Distance	$\bar{x} = x/a$	0.5 nm
Magnetic field (static)	$\bar{B}_0 = g\mu_B B_0 J/D^2$	≈0.07 T
Magnetic field (laser)	$\bar{B}_d = g\mu_B B_d/D$	≈0.78 T
Frequency (spin waves)	$\bar{\omega} = \hbar\omega J/D^2$	≈2.0 GHz
Frequency (laser)	$\tilde{\omega}_0 = \hbar\omega_0/J$	≈250 GHz

To describe the nonequilibrium steady state of the periodically driven magnetization, we employ the high-frequency Floquet-Magnus expansion [40] on the Landau-Lifshitz-Gilbert (LLG) equation and obtain the following effective Floquet Hamiltonian:

$$H_F = H_0 + \sum_{\boldsymbol{r}} g\mu_B B_F[-\hat{z}\cdot\boldsymbol{m}_{\boldsymbol{r}} + \mathcal{E}_d m_{\boldsymbol{r},z}m_{\boldsymbol{r},x} - \mathcal{E}_d^2(-2m_{\boldsymbol{r},x}^2 + m_{\boldsymbol{r},y}^2)\hat{z}\cdot\boldsymbol{m}_{\boldsymbol{r}}], \tag{4}$$

where $B_F = \{\gamma B_d^2\cos\delta/[2(1+\alpha^2)\omega_0]\}$ with γ the gyromagnetic ratio and α the Gilbert damping constant, and $\mathcal{E}_d = \lambda c/g\mu_B$ (Supplemental Material [47]). The second term corresponds to the effective magnetic field [19,20,40,71], while the third and fourth terms arise from the magnetoelectric nature of Cu_2OSeO_3. Below we show how these terms give rise to a novel control of the topology in real and reciprocal space.

Laser-driven skyrmion motion.—Since the x component of the magnetization changes sign across the center of

skyrmions, the third term of Eq. (4), obtained for $\mathbf{B}_0 \| [110]$, induces a dipolelike distortion in the spin texture [47]. Crucially, the induced distortion breaks the skyrmions' rotational symmetry, thus allowing for their laser-driven motion.

First we consider the dynamics of a single skyrmion under LCP light. We numerically solve the LLG equation obtained from the time-dependent Hamiltonian in Eq. (1) [47]. The motion of a single skyrmion is tracked by computing its center, defined as $R_i = \int d\boldsymbol{r}^2 \rho(\boldsymbol{r}) r_i / Q$ for $i = x, y$ with $\rho(\boldsymbol{r})$ and $Q = \int d\boldsymbol{r}^2 \rho(\boldsymbol{r})$ denoting the topological charge density and total topological charge, respectively [72].

The change in R_x and R_y as functions of time after irradiation of LCP light is shown in Fig. 2. Orienting $\mathbf{B}_0$ along other crystallographic directions induces different local electric dipole moments [42,43,47]. We find that the skyrmion under $\mathbf{B}_0 \| [110]$ exhibits translational motion along the negative y axis and a small drift velocity along the negative x axis, hence the skyrmion motion is mostly directed antiparallel to the net electric polarization. In contrast, the results for $\mathbf{B}_0 \| [001], [111]$ show no net displacement with almost identical trajectories. This is consistent with the symmetry argument, since the time-averaged spin textures for $\mathbf{B}_0 \| [001]$ and $\mathbf{B}_0 \| [111]$ respectively display C_{2z} and C_{3z} rotational symmetry, while no in-plane rotational symmetry is present for $\mathbf{B}_0 \| [110]$ [47].

We then combine the Floquet-Magnus expansion [40] with Thiele's approach to derive the analytical expression of the skyrmions' drift velocity $\boldsymbol{v}$ [26,74]. Up to first order in the Floquet-Magnus expansion, we obtain

$$v_x \approx -\frac{\alpha\eta}{4\pi Q} v_y,$$
$$v_y \approx -\frac{2.25}{Q} v_0 \bar{B}_F \mathcal{E}_d \alpha, \tag{5}$$

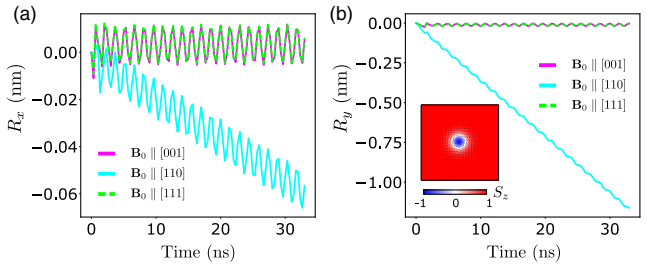

FIG. 2. Skyrmion motion under a circularly polarized laser. (a), (b) Displacement of the center of skyrmions (a) R_x and (b) R_y under LCP light as a function of time, defined in the text. The result for $\mathbf{B}_0 \| [001]$, $\mathbf{B}_0 \| [110]$, and $\mathbf{B}_0 \| [111]$ is respectively depicted in solid magenta, solid cyan, and dashed lime lines. The nonlinear effect of damping and asymmetric magnetoelectric coupling drive skyrmions without exciting internal magnon modes. The parameters are fixed as $D/J = 0.09$, $\bar{B}_0 = 0.9$, $\tilde{B}_d = 2.0$, $\tilde{\omega}_0 = 10$, $\mathcal{E}_d = 0.1$, and $\alpha = 0.04$ (see Table I). The inset in (b) shows the initial configuration of a single skyrmion prepared by Monte Carlo annealing for 150×150 spins [73].

where $\eta \approx 4\pi$ depends on the skyrmions spatial profile, $v_0 = a\gamma D^2 / g\mu_B J \approx 6.16$ m/s is a characteristic velocity, and $\bar{B}_F = g\mu_B B_F J / D^2$ is the dimensionless effective magnetic field. It is important to note that the drift velocity is in general proportional to the damping constant for an arbitrary local dipole moment $P_{\boldsymbol{r},i} = \chi^i_{jk} m_{\boldsymbol{r},j} m_{\boldsymbol{r},k}$ with $i, j, k = x, y, z$ [47]. Hence, damping is essential for the off-resonant skyrmion motion, where no internal magnon modes are excited due to the large difference between the laser THz-range frequency and the skyrmion magnon eigenfrequencies.

From Fig. 2, the velocity for $\mathbf{B}_0 \| [110]$ is estimated as $(v_x, v_y) = (-0.17\ \text{cm/s}, -3.52\ \text{cm/s})$. In comparison, Eq. (5) gives $(v_x, v_y) = (-0.088\ \text{cm/s}, -2.22\ \text{cm/s})$ for $Q = -1$ and $\eta = 4\pi$. On the other hand, the equivalent calculation for $\mathbf{B}_0 \| [001], [111]$ yields $\boldsymbol{v} = 0$ for the leading order term proportional to ω_0^{-1} [47]. Hence, our analytical expression is consistent with the LLG simulations. The dependence of v_y for $\mathbf{B}_0 \| [110]$ on B_d, $\mathcal{E}_d$, ω_0, and α is discussed in detail in [47], which is shown to be in a good agreement with Eq. (5) for small B_d and large ω_0, where the asymptotic behavior is described by the high-frequency expansion. Furthermore, our simulations confirm the skyrmion motion under ultrashort pulses [47] and reversal of skyrmion direction with switching from LCP light to RCP light, which changes the sign of B_F. We have demonstrated that the amplitude, frequency, and chirality of the laser affect the off-resonant motion of skyrmions, thus providing a greater control on their velocity, which can achieve a maximum of 15 cm/s [47].

Floquet magnonic topological phase transition.—On top of the applied static field B_0, circularly polarized laser irradiation generates an effective magnetic field B_F, which can be tuned by the laser field amplitude B_d. Therefore, analogously to the static magnetic-field driven topological phase transition in skyrmion crystals [33], we show that a Floquet magnonic topological phase transition can be driven by a circularly polarized laser.

Using the LLG equation, we study the magnetic excitations of a nonequilibrium steady-state skyrmion crystal sustained by RCP laser irradiation. We introduce, in addition to the laser field, pulsed magnetic fields along the in-plane and out-of-plane directions, which excite magnetically active skyrmion crystal spin wave modes [44]. The resonance frequencies of these modes are obtained from the dynamical susceptibilities [44,46] $\text{Im}\chi_{ij}(\omega) = M_{\omega,i}/B_{\omega,j}$, with $M_{\omega,i}$ and $B_{\omega,j}$ denoting the Fourier transform of the total magnetization $\boldsymbol{M}(t)$ and $\mathbf{B}(t)$ for $i, j = x, y, z$ [47].

Figure 3(a) shows $\text{Im}\chi_{xx}$ (blue) and $\text{Im}\chi_{zz}$ (red), where the resonance peaks of the counterclockwise (CCW), breathing, and clockwise (CW) modes are labeled as A, B, and C, respectively. These low-energy modes are similar to those obtained in static systems [44]. Additionally, a mode is found at $\bar{\omega} \approx 10.8$ in $\text{Im}\chi_{zz}$ as illustrated in the inset of Fig. 3(a). This high-energy mode is expected from the

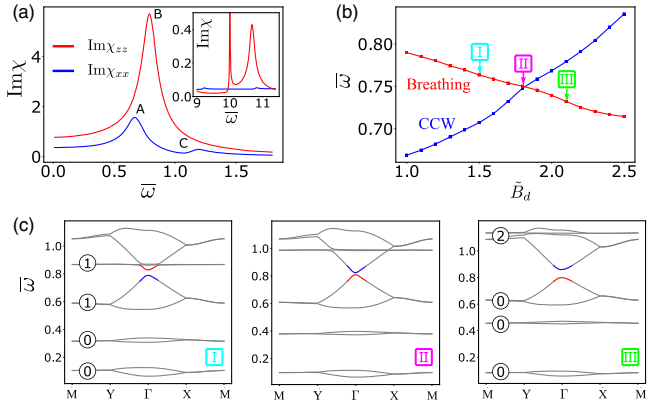

FIG. 3. Floquet magnonic topological phase transition in skyrmion crystals. (a) Imaginary parts of in-plane (out-of-plane) dynamical susceptibilities shown in blue (red), obtained at $D/J = 1.0$, $\bar{B}_0 = 0.4$, $\tilde{B}_d = 1.0$, $\tilde{\omega}_0 = 10$, $\mathcal{E}_d = 0.1$, and $\alpha = 0.04$ under RCP light. The resonance peaks of the (A) counterclockwise (CCW), (B) breathing, and (C) clockwise (CW) modes are indicated. The inset shows the result near the driving frequency $\tilde{\omega}_0 = 10$. (b) Resonance frequencies of the CCW (blue) and breathing (red) modes as functions of the laser field amplitude $\tilde{B}_d$. (c) Floquet magnon band structures in the vicinity of the topological phase transition with integers indicating the total Chern number for each group of bands. The CCW and breathing modes at the Γ points are highlighted in blue and red, respectively. Roman numerals in (b) mark the values of $\tilde{B}_d$ used in the panels in (c).

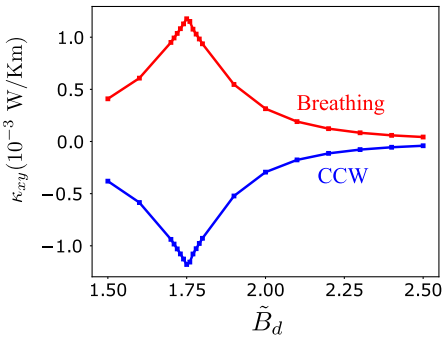

FIG. 4. Diagnosing a Floquet magnonic topological phase transition via the magnonic thermal Hall effect. The magnonic thermal Hall conductivity of the CCW (blue) and breathing (red) modes plotted against the laser field amplitude. These two modes can be resonantly and selectively excited using ac magnetic fields. The opposite sign enhancement at the critical value, due to the divergence of the Berry curvature, can be used as a topological phase transition diagnostic tool. The parameters are the same as in Fig 3(b).

periodic structure of the quasienergy spectrum given by $\epsilon_{nm} = \epsilon_n + m\hbar\omega_0$ for eigenvalues ϵ_n of the effective Floquet Hamiltonian and integers n, m [75]. We should note that the large, sharp peak at $\omega = \omega_0$ in $\mathrm{Im}\chi_{zz}$ corresponds to the laser field, while the signal from $\mathrm{Im}\chi_{xx}$ is too weak to observe any peaks near $\omega = \omega_0$.

The resonance frequencies of the CCW (blue) and breathing (red) modes as functions of $\tilde{B}_d$ are shown in Fig. 3(b), from where we identify the band inversion point at the critical value $\tilde{B}_d \approx 1.8$. The total effective magnetic field at this point is estimated as $\bar{B}_F + \bar{B}_0 \approx 0.56$. Remarkably, it is almost equal to the critical magnetic field obtained in static systems [33] and thus consistent with Floquet magnons experiencing a laser-induced effective field. We find that the critical value of the total effective magnetic field remains roughly constant up to $\tilde{\omega}_0 \geq 5$, where the high-frequency expansion is justified [47].

Treating the time-averaged spin configuration of the nonequilibrium steady state as the classical spin ground state for the effective Floquet Hamiltonian in Eq. (4), we compute the Floquet magnon band structures (see [47]) shown in Fig. 3(c). The laser-driven Floquet magnonic topological phase transition is signaled by the closing of the gap between the CCW and breathing modes, at the band inversion point, with the consequent Chern number transfer. The obtained Floquet magnon band structures are consistent with the LLG simulation results. We note that the topological phase transition occurs at a slightly smaller $\tilde{B}_d$ value in the Floquet magnon band structures, which may arise from higher order terms neglected in the Floquet Hamiltonian. Invoking the bulk-boundary correspondence, the above Chern number transfer opens the door to laser-controlled switching of nonreciprocal Floquet magnonic chiral edge states due to the magnetoelectric coupling [47].

As a bulk probe for the laser-driven topological phase transition, we consider the Floquet magnonic thermal Hall conductivity [36–38,76]

$$\kappa_{xy} = -\frac{k_B^2 T}{\hbar d} \sum_n \int \frac{d^2\boldsymbol{k}}{(2\pi)^2} c_2(\rho_{n,\boldsymbol{k}}) \Omega_n(\boldsymbol{k}), \tag{6}$$

where d is the interlayer distance, $\Omega_n(\boldsymbol{k})$ is the Berry curvature of the nth Floquet magnon band, $\rho_{n,\boldsymbol{k}}$ is the distribution function of the nth Floquet magnon eigenstate at $\boldsymbol{k}$, and $c_2(\rho) = (1+\rho)\{\log[(1+\rho)/\rho]\}^2 - (\log\rho)^2 - 2\mathrm{Li}_2(-\rho)$ with $\mathrm{Li}_2(z)$ denoting the polylogarithm function of order two. While the population of magnons in the CCW (breathing) mode is small at thermal equilibrium, we could selectively pump them with in-plane (out-of-plane) ac magnetic fields [31,44,77]. In this resonance condition, we can approximate $\rho_{n,\boldsymbol{k}}$ with a Gaussian distribution sharply peaked at the Γ point of the corresponding magnon band [47]. Crucially, the thermal Hall conductivity from the resonant CCW (breathing) mode is strongly enhanced due to the divergence of the Berry curvature at the topological phase transition. Figure 4 clearly illustrates the enhancement with opposite sign for the CCW and breathing modes, obtained for a thin film sample of Cu_2OSeO_3 with $d = 1$ nm and $T = 5$ K [41].

Conclusion.—We have established a novel formalism to describe laser-controlled topology in real and reciprocal

space of multiferroic insulators. Crucially, our theory incorporates the phenomenological damping effect to the Floquet magnon formalism, which is essential in a nonequilibrium condition under driving fields. Taking Cu_2OSeO_3 as a model, we have demonstrated the off-resonance motion of skyrmions due to the magnetoelectric effect. We have also shown that circularly polarized lasers induce a Floquet magnonic topological phase transition. Furthermore, exploiting the selection rules of CCW and breathing modes of skyrmion crystals [31,44,77], we have suggested the magnonic thermal Hall conductivity as a diagnostic tool for the topological phase transition. Our formalism can be generalized to other multiferroics such as GaV_4S_8 [78,79]. The ultrafast control of topological spin structures and Floquet magnon band topology in multiferroic insulators broadens the spectrum of potential spintronic and magnonic applications.

We are grateful to T. Hinokihara, H. Matsuura, and M. Ogata for discussions. We also thank S. Seki and A. Mook for their insightful advice on the magnonic thermal Hall effect in skyrmion crystals. T. H. is supported by Japan Society for the Promotion of Science (JSPS) through Program for Leading Graduate Schools (MERIT) and JSPS KAKENHI (Grant No. 18J21985). This work was supported by the Swiss National Science Foundation and NCCR QSIT. This project received funding from the European Union's Horizon 2020 research and innovation program (ERC Starting Grant, Grant Agreement No. 757725).

[1] Y. Tserkovnyak, A. Brataas, G. E. W. Bauer, and B. I. Halperin, Nonlocal magnetization dynamics in ferromagnetic heterostructures, Rev. Mod. Phys. **77**, 1375 (2005).
[2] S. S. P. Parkin, M. Hayashi, and L. Thomas, Magnetic domain-wall racetrack memory, Science **320**, 190 (2008).
[3] F. Jonietz, S. Mühlbauer, C. Pfleiderer, A. Neubauer, W. Münzer, A. Bauer, T. Adams, R. Georgii, P. Böni, R. A. Duine, K. Everschor, M. Garst, and A. Rosch, Spin transfer torques in MnSi at ultralow current densities, Science **330**, 1648 (2010).
[4] A. Fert, V. Cros, and J. Sampaio, Skyrmions on the track, Nat. Nanotechnol. **8**, 152 (2013).
[5] K. A. van Hoogdalem, Y. Tserkovnyak, and D. Loss, Magnetic texture-induced thermal Hall effects, Phys. Rev. B **87**, 024402 (2013).
[6] R. Shindou, R. Matsumoto, S. Murakami, and J. I. Ohe, Topological chiral magnonic edge mode in a magnonic crystal, Phys. Rev. B **87**, 174427 (2013).
[7] L. Zhang, J. Ren, J. S. Wang, and B. Li, Topological magnon insulator in insulating ferromagnet, Phys. Rev. B **87**, 144101 (2013).
[8] K. Nakata, J. Klinovaja, and D. Loss, Magnonic quantum Hall effect and Wiedemann-Franz law, Phys. Rev. B **95**, 125429 (2017).
[9] K. Nakata, S. K. Kim, J. Klinovaja, and D. Loss, Magnonic topological insulators in antiferromagnets, Phys. Rev. B **96**, 224414 (2017).
[10] A. V. Chumak, V. I. Vasyuchka, A. A. Serga, and B. Hillebrands, Magnon spintronics, Nat. Phys. **11**, 453 (2015).
[11] A. Mook, S. A. Díaz, J. Klinovaja, and D. Loss, Chiral hinge magnons in second-order topological magnon insulators, Phys. Rev. B **104**, 024406 (2021).
[12] B. Trauzettel, P. Simon, and D. Loss, Ac Magnetization Transport and Power Absorption in Nonitinerant Spin Chains, Phys. Rev. Lett. **101**, 017202 (2008).
[13] K. N. Tu, Y. Liu, and M. Li, Effect of Joule heating and current crowding on electromigration in mobile technology, Appl. Phys. Rev. **4**, 011101 (2017).
[14] G. Tatara, H. Kohno, and J. Shibata, Microscopic approach to current-driven domain wall dynamics, Phys. Rep. **468**, 213 (2008).
[15] A. Kirilyuk, A. V. Kimel, and T. Rasing, Ultrafast optical manipulation of magnetic order, Rev. Mod. Phys. **82**, 2731 (2010).
[16] E. Beaurepaire, J.-C. Merle, A. Daunois, and J.-Y. Bigot, Ultrafast Spin Dynamics in Ferromagnetic Nickel, Phys. Rev. Lett. **76**, 4250 (1996).
[17] A. V. Kimel, A. Kirilyuk, P. A. Usachev, R. V. Pisarev, A. M. Balbashov, and T. Rasing, Ultrafast non-thermal control of magnetization by instantaneous photomagnetic pulses, Nature (London) **435**, 655 (2005).
[18] T. Kampfrath, A. Sell, G. Klatt, A. Pashkin, S. Mährlein, T. Dekorsy, M. Wolf, M. Fiebig, A. Leitenstorfer, and R. Huber, Coherent terahertz control of antiferromagnetic spin waves, Nat. Photonics **5**, 31 (2011).
[19] S. Takayoshi, M. Sato, and T. Oka, Laser-induced magnetization curve, Phys. Rev. B **90**, 214413 (2014).
[20] S. Takayoshi, H. Aoki, and T. Oka, Magnetization and phase transition induced by circularly polarized laser in quantum magnets, Phys. Rev. B **90**, 085150 (2014).
[21] I. E. Dzyaloshinskii, On the magneto-electrical effect in antiferromagnets, Sov. Phys. JETP **10**, 628 (1960), http://jetp.ras.ru/cgi-bin/e/index/e/10/3/p628?a=list.
[22] T. Kimura, T. Goto, H. Shintani, K. Ishizaka, T. Arima, and Y. Tokura, Magnetic control of ferroelectric polarization, Nature (London) **426**, 55 (2003).
[23] T. Arima, Spin-driven ferroelectricity and magneto-electric effects in frustrated magnetic systems, J. Phys. Soc. Jpn. **80**, 052001 (2011).
[24] M. Sato, S. Takayoshi, and T. Oka, Laser-Driven Multiferroics and Ultrafast Spin Current Generation, Phys. Rev. Lett. **117**, 147202 (2016).
[25] N. Nagaosa and Y. Tokura, Topological properties and dynamics of magnetic skyrmions, Nat. Nanotechnol. **8**, 899 (2013).
[26] W. Wang, M. Beg, B. Zhang, W. Kuch, and H. Fangohr, Driving magnetic skyrmions with microwave fields, Phys. Rev. B **92**, 020403(R) (2015).
[27] M. Ikka, A. Takeuchi, and M. Mochizuki, Resonance modes and microwave-driven translational motion of a skyrmion crystal under an inclined magnetic field, Phys. Rev. B **98**, 184428 (2018).
[28] A. Takeuchi and M. Mochizuki, Selective activation of an isolated magnetic skyrmion in a ferromagnet with microwave electric fields, Appl. Phys. Lett. **113**, 072404 (2018).

[29] H. Y. Yuan, X. S. Wang, M.-H. Yung, and X. R. Wang, Wiggling skyrmion propagation under parametric pumping, Phys. Rev. B **99**, 014428 (2019).
[30] A. Roldn-Molina, A. S. Nunez, and J. Fernndez-Rossier, Topological spin waves in the atomic-scale magnetic skyrmion crystal, New J. Phys. **18**, 045015 (2016).
[31] M. Garst, J. Waizner, and D. Grundler, Collective spin excitations of helices and magnetic skyrmions: Review and perspectives of magnonics in non-centrosymmetric magnets, J. Phys. D **50**, 293002 (2017).
[32] S. A. Díaz, J. Klinovaja, and D. Loss, Topological Magnons and Edge States in Antiferromagnetic Skyrmion Crystals, Phys. Rev. Lett. **122**, 187203 (2019).
[33] S. A. Díaz, T. Hirosawa, J. Klinovaja, and D. Loss, Chiral magnonic edge states in ferromagnetic skyrmion crystals controlled by magnetic fields, Phys. Rev. Research **2**, 013231 (2020).
[34] T. Hirosawa, S. A. Díaz, J. Klinovaja, and D. Loss, Magnonic Quadrupole Topological Insulator in Antiskyrmion Crystals, Phys. Rev. Lett. **125**, 207204 (2020).
[35] A. Mook, J. Klinovaja, and D. Loss, Quantum damping of skyrmion crystal eigenmodes due to spontaneous quasiparticle decay, Phys. Rev. Research **2**, 033491 (2020).
[36] Y. Onose, T. Ideue, H. Katsura, Y. Shiomi, N. Nagaosa, and Y. Tokura, Observation of the magnon Hall effect, Science **329**, 297 (2010).
[37] H. Katsura, N. Nagaosa, and P. A. Lee, Theory of the Thermal Hall Effect in Quantum Magnets, Phys. Rev. Lett. **104**, 066403 (2010).
[38] R. Matsumoto and S. Murakami, Theoretical Prediction of a Rotating Magnon Wave Packet in Ferromagnets, Phys. Rev. Lett. **106**, 197202 (2011).
[39] T. L. Gilbert, A phenomenological theory of damping in ferromagnetic materials, IEEE Trans. Magn. **40**, 3443 (2004).
[40] S. Higashikawa, H. Fujita, and M. Sato, Floquet engineering of classical systems, arXiv:1810.01103.
[41] S. Seki, X. Z. Yu, S. Ishiwata, and Y. Tokura, Observation of skyrmions in a multiferroic material, Science **336**, 198 (2012).
[42] S. Seki, S. Ishiwata, and Y. Tokura, Magnetoelectric nature of skyrmions in a chiral magnetic insulator Cu_2OSeO_3, Phys. Rev. B **86**, 060403(R) (2012).
[43] M. Mochizuki and S. Seki, Dynamical magnetoelectric phenomena of multiferroic skyrmions, J. Phys. Condens. Matter **27**, 503001 (2015).
[44] M. Mochizuki, Spin-Wave Modes and Their Intense Excitation Effects in Skyrmion Crystals, Phys. Rev. Lett. **108**, 017601 (2012).
[45] M. Mochizuki and S. Seki, Magnetoelectric resonances and predicted microwave diode effect of the skyrmion crystal in a multiferroic chiral-lattice magnet, Phys. Rev. B **87**, 134403 (2013).
[46] M. Mochizuki, Microwave Magnetochiral Effect in Cu_2OSeO_3, Phys. Rev. Lett. **114**, 197203 (2015).
[47] See Supplemental Material at http://link.aps.org/supplemental/10.1103/PhysRevLett.128.037201 for details of the LLG equation; electric polarization of Cu_2OSeO_3; Floquet theory for classical spin dynamics; effective Floquet Hamiltonian; velocity of laser-driven skyrmion motion; spin wave excitations under laser fields; Floquet magnon Hamiltonian; laser-controlled chiral magnonic edge states; Floquet magnonic thermal Hall conductivity; laser parameters and heating effect; skyrmion motion under ultrashort laser pulses, which includes Refs. [48–70].
[48] T. Arima, Ferroelectricity induced by proper-screw type magnetic order, J. Phys. Soc. Jpn. **76**, 073702 (2007).
[49] Y. Takahashi, R. Shimano, Y. Kaneko, H. Murakawa, and Y. Tokura, Magnetoelectric resonance with electromagnons in a perovskite helimagnet, Nat. Phys. **8**, 121 (2012).
[50] D. Hüvonen, U. Nagel, T. Rõõm, Y. J. Choi, C. L. Zhang, S. Park, and S.-W. Cheong, Magnetic excitations and optical transitions in the multiferroic spin-$\frac{1}{2}$ system $LiCu_2O_2$, Phys. Rev. B **80**, 100402(R) (2009).
[51] J. L. Mateos, Chaotic Transport and Current Reversal in Deterministic Ratchets, Phys. Rev. Lett. **84**, 258 (2000).
[52] I. Zapata, S. Albaladejo, J. M. R. Parrondo, J. J. Sáenz, and F. Sols, Deterministic Ratchet from Stationary Light Fields, Phys. Rev. Lett. **103**, 130601 (2009).
[53] Y. H. Liu, Y. Q. Li, and J. H. Han, Skyrmion dynamics in multiferroic insulators, Phys. Rev. B **87**, 100402(R) (2013).
[54] C. Psaroudaki and D. Loss, Skyrmions Driven by Intrinsic Magnons, Phys. Rev. Lett. **120**, 237203 (2018).
[55] Y. Aharonov and A. Casher, Topological Quantum Effects for Neutral Particles, Phys. Rev. Lett. **53**, 319 (1984).
[56] S. A. Owerre, Magnonic Floquet Hofstadter butterfly, Ann. Phys. (Amsterdam) **399**, 93 (2018).
[57] K. Nakata, S. K. Kim, and S. Takayoshi, Laser control of magnonic topological phases in antiferromagnets, Phys. Rev. B **100**, 014421 (2019).
[58] M. Elyasi, K. Sato, and G. E. W. Bauer, Topologically nontrivial magnonic solitons, Phys. Rev. B **99**, 134402 (2019).
[59] N. del Ser, L. Heinen, and A. Rosch, Archimedean screw in driven chiral magnets, SciPost Phys. **11**, 9 (2021).
[60] T. Oka and S. Kitamura, Floquet engineering of quantum materials, Annu. Rev. Condens. Matter Phys. **10**, 387 (2019).
[61] J. H. P. Colpa, Diagonalization of the quadratic boson hamiltonian, Physica (N.Y.) **93A**, 327 (1978).
[62] K. Nakata, P. Simon, and D. Loss, Magnon transport through microwave pumping, Phys. Rev. B **92**, 014422 (2015).
[63] L. Rózsa, J. Hagemeister, E. Y. Vedmedenko, and R. Wiesendanger, Effective damping enhancement in noncollinear spin structures, Phys. Rev. B **98**, 100404(R) (2018).
[64] A. Pashkin, F. Junginger, B. Mayer, C. Schmidt, O. Schubert, D. Brida, R. Huber, and A. Leitenstorfer, Quantum physics with ultrabroadband and intense terahertz pulses, IEEE J. Sel. Top. Quantum Electron. **19**, 8401608 (2013).
[65] J. A. Fülöp, S. Tzortzakis, and T. Kampfrath, Laser-driven strong-field terahertz sources, Adv. Opt. Mater. **8**, 1900681 (2020).
[66] R. B. Versteeg, I. Vergara, S. D. Schäfer, D. Bischoff, A. Aqeel, T. T. M. Palstra, M. Grüninger, and P. H. M. van Loosdrecht, Optically probed symmetry breaking in the chiral magnet Cu_2OSeO_3, Phys. Rev. B **94**, 094409 (2016).
[67] N. Ogawa, S. Seki, and Y. Tokura, Ultrafast optical excitation of magnetic skyrmions, Sci. Rep. **5**, 9552 (2015).

[68] J. W. McIver, B. Schulte, F.-U. Stein, T. Matsuyama, G. Jotzu, G. Meier, and A. Cavalleri, Light-induced anomalous Hall effect in graphene, Nat. Phys. **16**, 38 (2020).

[69] K. Toyota, U. Saalmann, and J. M. Rost, The envelope Hamiltonian for electron interaction with ultrashort pulses, New J. Phys. **17**, 073005 (2015).

[70] L. Medišauskas, U. Saalmann, and J. M. Rost, Floquet Hamiltonian approach for dynamics in short and intense laser pulses, J. Phys. B **52**, 015602 (2019).

[71] M. Miyake and M. Mochizuki, Creation of nanometric magnetic skyrmions by global application of circularly polarized microwave magnetic field, Phys. Rev. B **101**, 094419 (2020).

[72] B. Berg and M. Lüscher, Definition and statistical distributions of a topological number in the lattice O(3) σ-model, Nucl. Phys. **B190**, 412 (1981).

[73] R. F. L. Evans, W. J. Fan, P. Chureemart, T. A. Ostler, M. O. A. Ellis, and R. W. Chantrell, Atomistic spin model simulations of magnetic nanomaterials, J. Phys. Condens. Matter **26**, 103202 (2014).

[74] A. A. Thiele, Steady-State Motion of Magnetic Domains, Phys. Rev. Lett. **30**, 230 (1973).

[75] A. Eckardt and E. Anisimovas, High-frequency approximation for periodically driven quantum systems from a Floquet-space perspective, New J. Phys. **17**, 093039 (2015).

[76] S. A. Owerre, Floquet topological magnons, J. Phys. Commun. **1**, 021002 (2017).

[77] Y. Onose, Y. Okamura, S. Seki, S. Ishiwata, and Y. Tokura, Observation of Magnetic Excitations of Skyrmion Crystal in a Helimagnetic Insulator Cu_2OSeO_3, Phys. Rev. Lett. **109**, 037603 (2012).

[78] I. Kézsmárki, S. Bordács, P. Milde, E. Neuber, L. M. Eng, J. S. White, H. M. Rnnow, C. D. Dewhurst, M. Mochizuki, K. Yanai, H. Nakamura, D. Ehlers, V. Tsurkan, and A. Loidl, Néel-type skyrmion lattice with confined orientation in the polar magnetic semiconductor GaV_4S_8, Nat. Mater. **14**, 1116 (2015).

[79] E. Ruff, S. Widmann, P. Lunkenheimer, V. Tsurkan, S. Bordács, I. Kézsmárki, and A. Loidl, Multiferroicity and skyrmions carrying electric polarization in GaV_4S_8, Sci. Adv. **1**, e1500916 (2015).